Decomposing Neuroanatomical Heterogeneity of Autism Spectrum Disorder Across Different Developmental Stages Using Morphological Multiplex Network Model

Xiang Fu, Ying Wang, Jialong Li, Hongmin Cai, *Senior Member, IEEE*, Xinyan Zhang, Zhijun Yao, *Member, IEEE*, Minqiang Yang, *Member, IEEE*, and Weihao Zheng, *Member, IEEE*

***Abstract*—Autism spectrum disorder (ASD) is accompanied by impaired social cognition and behavior. The expense of supporting patients with ASD turns into a significant problem for society. Parsing neurobiological subtypes is a crucial way for delineating the heterogeneity in autistic brains, with significant implications for improving ASD diagnosis and promoting the development of personalized intervention models. Nevertheless, a comprehensive understanding of the heterogeneity in cortical morphology of ASD is still lacking, and the question of whether neuroanatomical subtypes remain stable during cortical development remains unclear. Here, we used T1-weighted images of 515 male patients with ASD, including 216 autistic children (6–11 years), 187 adolescents (12–17 years), and 112 young adults (18–29 years), along with 595 age and gender-matched typically developing (TD) individuals. Cortical thickness (CT), surface area (SA), and volumes of cortical (CV) and subcortical (SV) regions were extracted. A single network layer was established by calculating the covariance of each feature across brain regions between participants, thereby constructing a multilayer intersubject covariance network. Applying a community detection algorithm to multilayer networks derived from different feature combinations, we observed that the network comprising CT and CV layers exhibited the most prominent modular organization, resulting in three subtypes of ASD for each of the three age groups. Subtypes within the corresponding age group significantly differed in terms of brain morphology and clinical scales. Furthermore, the subtypes of children with ASD underwent reorganization with development, transitioning from childhood to adolescence and adulthood, rather than consistently persist. Additionally, subtype categorization largely improved the diagnostic accuracy of ASD compared to diagnosing the entire ASD cohort. These findings demonstrated distinct neuroanatomical manifestations of ASD subtypes across various developmental periods, highlighting the significance of age-related subtyping in facilitating the etiology and diagnosis of ASD.**

***Index Terms*—Age-related subtyping, autism spectrum disorder (ASD), diagnosis, multilayer network, neuroanatomical heterogeneity.**

I. Introduction

AUTISM spectrum disorder (ASD) has a serious impact on the social lives of patients, and also increases the medical burden of society heavily [1]. ASD is a pervasive neurodevelopmental disorder characterized by social dysfunction, restricted interests, and stereotyped and repetitive behaviors [2]. Individuals with ASD often exhibit comorbidities such as attention deficit hyperactivity disorder (ADHD), language and behavior disorders, anxiety, depression, and developmental delays [2], [3], [4]. Currently, the diagnosis of such disorders relies heavily on clinical assessments and interviews, which are inherently subjective and highly dependent on the experiences of clinicians [5], [6]. Moreover, the heterogeneity observed in clinical and behavioral manifestations of patients with ASD poses a significant challenge to the understanding and treatment of this condition [7]. In addition, the issue of inaccurate ASD diagnosis stemming from the heterogeneity remains unresolved. Therefore, there is a pressing need to explore the neurobiological mechanisms underpinning the clinical heterogeneity present in ASD patients to deepen understanding and improve the diagnosis of ASD.

Structural magnetic resonance imaging (MRI) is a noninvasive tissue imaging technique with high spatial resolution and has been extensively employed for depicting brain anatomy [8], [9], [10]. Previous studies have highlighted atypical brain overgrowth [11], [12], [13], [14] and an expansion of cortical surface area (SA) [15] in young children with ASD. The termination of brain overgrowth occurred at a later developmental stage [16], [17], [18], followed by a sustained and accelerated thinning of

Manuscript received 8 March 2024; revised 28 April 2024; accepted 3 June 2024. Date of publication 26 June 2024; date of current version 2 October 2024. This work was supported in part by the National Natural Science Foundation of China under Grant U21A20520, Grant 62202212, and Grant 62227807; in part by the STI2030-Major Projects under Grant 2021ZD0202002 and Grant 2021ZD0200800; in part by the National Key Research and Development Program of China under Grant 2019YFA0706200; and in part by the Science and Technology Program of Gansu Province under Grant 23YFGA0004 and Grant 23JRRA1136. *(Corresponding authors: Minqiang Yang; Weihao Zheng).*

Xiang Fu, Ying Wang, Jialong Li, Xinyan Zhang, Zhijun Yao, Minqiang Yang, and Weihao Zheng are with Gansu Provincial Key Laboratory of Wearable Computing, School of Information Science and Engineering, Lanzhou University, Lanzhou 730000, China (e-mail: fux2019@lzu.edu.cn; wangying22@lzu.edu.cn; 220220942951@lzu.edu.cn; 120220909261@lzu.edu.cn; yaozj@lzu.edu.cn; yangmq@lzu.edu.cn; zhengweihao@lzu.edu.cn).

Hongmin Cai is with the School of Computer Science and Engineering, South China University of Technology, Guangzhou 510641, China (e-mail: hmcai@scut.edu.cn).

This article has supplementary downloadable material available at https://doi.org/10.1109/TCSS.2024.3411113, provided by the authors.

Digital Object Identifier 10.1109/TCSS.2024.3411113

the cerebral cortex in adulthood [19], [20]. Some other studies reported opposite results, for example, patients with ASD demonstrated widespread increases in cortical thickness (CT) from late childhood to adulthood relative to typical development (TD) [21]; however, the topological organization of CT exhibited fewer abnormalities than that observed in SA across this developmental period [22]. On the other hand, although plenty of evidence posits abnormalities in the cortical anatomy of individuals with ASD, morphological metrics showed limited diagnostic power for ASD [23], [24]. One predominant reason for the inconsistent findings may be attributed to the existence of neurobiological subtypes in ASD. Each subtype exhibits unique clinical phenotypes and neuroanatomical manifestations [25], [26], [27], thereby limiting the generalizability and reproducibility of these studies. Therefore, it is imperative to thoroughly delineate the heterogeneity of cerebral anatomy in ASD by using multiple morphological features and spanning various developmental stages.

Recent studies have made significant progress in decomposing heterogeneity in autistic brains by identifying more homogeneous subgroups using unsupervised clustering algorithms. For example, morphological measurements (such as CT and brain volume) were used for identifying structural subtypes of ASD [28], [29]. Some researchers have used hierarchical clustering based on the volume of the corpus callosum, hippocampus, caudate, and amygdala to identify four ASD subtypes [28]. Another study found three ASD subtypes based on whole-brain voxel with k-means analysis [29]. In addition, there have been studies identifying ASD subtypes with resting fMRI [30], [31]. Researchers have identified significant linear combinations of resting-state connectomic and clinical profiles of ASD and applied hierarchical clustering to find three ASD subtypes [30]. Another study computed the interindividual deviation of functional connectivity of the functional connectivity of each ASD patient from that of the TD group to conduct a k-means algorithm to identify two subtypes [31]. Although methodologies vary, these previous researches have revealed evidence of at least two to four ASD subtypes [23], [25]. However, previous studies based on structural MRI primarily conducted unsupervised clustering on a single morphological feature, which omitted the diversified features of cortical morphology (e.g., SA, CT, CV, and SV), and therefore may not well characterize the neuroanatomical subgroups in patients with ASD.

Multiplex networks are multilayer systems that contain vertices linked across multiple interacting layers [32]. Layers of the network share the same vertices and are interconnected between the adjacent layers. Because the multilayer networks can better describe different types of interactions in a complex system, this technology has been utilized to study the connectomic mechanism in the brain. For example, a previous study constructed a two-layer network model by using the structural and functional networks, and reported that structural connectivity was assortative while functional connectivity was disassortative [33] and these findings reveal the advantage of multiplex networks in elucidating the complexity of brain networks; another study aggregated different features of the cortical surface shape into a morphological multiplex network, and used it to discriminate between late mild cognitive impairment and Alzheimer's disease with biomarkers of left and right cortical hemispheres, and obtained the best accuracy as 71.43% and 77.92% separately, which is much higher than that of the single layer network [34]. These findings suggested that multiple networks can better integrate the features of different dimensions, so as to better characterize structural and functional information of the brain [35]. Recognizing the advantages of the multiplex network model methodology, we adopted this to combine various morphological features to find a more reliable partition of the ASD subgroups.

This study aims to comprehensively delineate neuroanatomical subtypes in ASD brains by integrating multiple morphological features. The null hypothesis is ASD exhibits biological heterogeneity, and this heterogeneity changes with age. We categorized 515 ASD patients and 595 TD individuals into three age ranges, including childhood (6–11 years), adolescence (12–17 years), and young adulthood (18–29 years). For each age group, we built a multiplex network comprising multiple connectivity layers to represent interindividual relationships across multiple morphological features. A community detection algorithm for the multiplex network was used to decompose potential subgroups in brain morphology meanwhile considering the interlayer relationships. We evaluated the clustering performance by comparing clinical assessments and morphological features of each subgroup against the TD cohort, as well as between the subgroups. The distance between subtypes across different age ranges was also calculated to characterize the possible developmental trajectories of these subtypes. In addition, we employed multiple classifiers to examine the clinical utility of the neuroanatomical subtypes in facilitating ASD diagnosis.

II. Materials and Methods

A. Participants

T1-weighted images were downloaded from the Autism Brain Image Data Exchange database (ABIDE) (http://fcon_1000.projects.nitrc.org/indi/abide/). Detailed acquisition parameters are shown in Table S1. To enhance the reliability and repeatability of the findings, we implemented a data exclusion scheme. The exclusion criteria are as follows: 1) female participants; 2) participants who are older than 30 years; 3) participants without handedness information; 4) image quality did not meet the specified standards (refer to Section II-B); and 5) data from acquisition sites with less than 10 subjects (Table S2). The remaining participants were divided into three age groups: 216 children (6–11 years old), 187 adolescents (12–17 years), and 112 adults (18–29 years) [22], [36]. Detailed demographic and clinical information are given in Table I.

B. MRI Preprocessing

Imaging data were preprocessed using Freesurfer v7.2.0 (http://surfer.nmr.mgh.harvard.edu). Briefly, this procedure included nonuniform field strength and motion correction, coordinate transformation, tissue segmentation, and surface reconstruction [37], [38], [39]. The Euler number, which reflects the integrity of the polyhedron simulated by the brain, was used to

TABLE I
DEMOGRAPHIC INFORMATION OF THE PARTICIPANTS

Variables	Children (n = 494)			Adolescents (n = 373)			Adults (n = 243)		
N	ASD	TD	P	ASD	TD	P	ASD	TD	P
	216	278		187	186		112	131	
Age	9.58 ± 1.6	9.86 ± 1.3	0.028	14.29 ± 1.7	14.54 ± 1.8	0.179	21.48 ± 3.1	22.96 ± 3.3	<0.001
FIQ	107.32 ± 18.2	114.24 ± 12.7	<0.001	104.41 ± 15.9	109.97 ± 13.2	<0.001	110.32 ± 14.3	115.41 ± 10.0	0.001
VIQ	109.71 ± 19.4	116.48 ± 13.9	<0.001	104.29 ± 17.5	111.71 ± 13.9	<0.001	111.03 ± 14.2	114.76 ± 10.4	0.058
PIQ	106.63 ± 17.2	109.66 ± 14.1	0.055	102.84 ± 16.0	106.39 ± 13.03	0.029	108.63 ± 15.6	113.27 ± 11.9	0.028
ADOS_TOTAL	11.29 ± 3.8	-	-	10.99 ± 3.7	-	-	10.86 ± 3.6	1.88 ± 1.4	<0.001
ADOS_COMM	3.19 ± 1.6	-	-	3.52 ± 1.4	-	-	3.56 ± 1.4	1.25 ± 0.7	<0.001
ADOS_SOCIAL	7.86 ± 2.4	-	-	7.53 ± 3.0	-	-	7.28 ± 2.7	0.63 ± 1.1	<0.001
ADOS_STEREO_BEHAV	2.10 ± 1.5	-	-	1.48 ± 1.5	-	-	1.46 ± 1.4	0.19 ± 0.4	<0.001

There is no ADOS data in healthy children and adolescents. Counts of other scores: TOTAL (ASD children: 111, ASD adolescents: 92, ASD adults: 90, TD adults: 16); COMM (ASD children: 111, ASD adolescents: 77, ASD adults: 80, TD adults: 16); SOCIAL (ASD children: 111, ASD adolescents: 78, ASD adults: 80, TD adults: 16); STEREO_BEHAV (ASD children: 99, ASD adolescents: 66, ASD adults: 74, TD adults: 16).

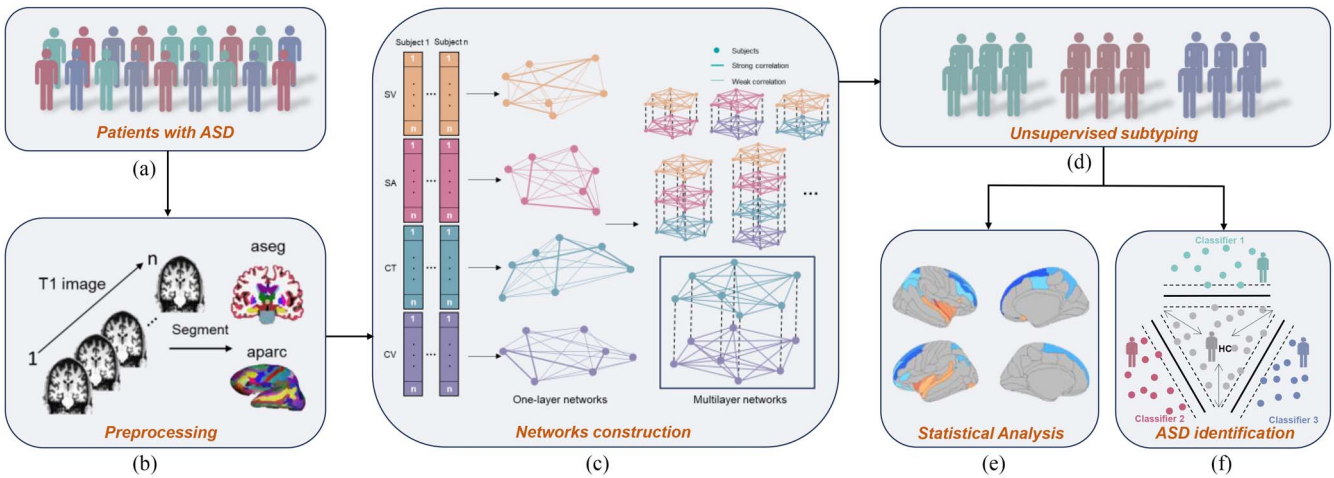

Fig. 1. Flowchart of data analysis. (a) Patients with ASD selected by exclusion criteria. (b) Image preprocessing and cortical parcellation according to the Destrieux atlas. (c) Multiplex network construction based on intersubject correlations of multiple morphological features (i.e., SA, CT, CV, and SV). The two-layer multiplex network framed represents the final selected networks constructed by CT and CV. (d) Community detection for the multiplex network. (e) Statistical analysis on morphology features and clinical scales. (f) Subtyping-based classification strategy for ASD diagnosis.

assess the image quality [40]. This metric was suggested to provide assessments of image quality that are comparable to those made by experienced researchers [40]. Images with Euler number of outliers (beyond plus or minus three standard deviations from the mean) were excluded [41].

Surfaces were inflated and registered to a prior template to calculate morphological measurements of the brain, including SA, CT, and CV [42], [43]. Each cortical surface was parcellated into 148 regions according to the Destrieux atlas [44], and SA, CT, and CV were computed for each region. We also calculated volumes of 12 subcortical nuclei (SV) defined based on the automatic segmentation (ASeg) atlas [45] [Fig. 1(b)].

C. Construction of Morphological Multiplex Networks

The morphological similarity between pairs of subjects was assessed using the Pearson correlation coefficient [Fig. 1(c)]. This analysis was conducted separately for each morphological feature (i.e., SA, CT, CV, and SV) to form an interindividual similarity matrix, serving as a single layer within the multiplex network. To explore the influence of feature selection, we constructed multiplex network models by using different combinations of morphological features. This process yielded six double-layer networks, four triple-layer networks, and one quadruple-layer network. The pipeline for network construction and analysis is shown in Fig. 1. Notably, the aforementioned process was performed independently for each age group, resulting in networks with varying numbers of nodes (n = 216, 187, and 112 for children, adolescents, and adults, respectively).

D. Community Detection

The Leiden algorithm was employed to identify communities within a multiplex network [46]. The Leiden algorithm is actually an improved version of the Louvain algorithm [47], which is faster and superior. Compared to the Louvain algorithm, the Leiden algorithm, ensures well-connected communities, offers faster execution due to its reliance on a quick local moving method, provides better partitioning results, and gives explicit guarantees that it will converge to a partition where all subsets

of all communities are optimally assigned when iteratively applied [46]. The evaluation index Q [48] of the Leiden algorithm is defined as follows:

$$Q = \frac{1}{2m}\sum_{ij}\left(A_{ij} - \frac{k_i k_j}{2m}\right)\delta(\sigma_i, \sigma_j) \quad (1)$$

where A is the adjacent matrix, k_i denotes the degree of vertex i, m is the number of edges, and σ_i is the community to which vertex i belongs ($\delta(\sigma_i, \sigma_j) = 1$ if $\sigma_i = \sigma_j$, and 0 otherwise). In the iterative process of a multiplex network, the Q value is initialized and then optimized by moving nodes between communities to maximize the modularity gain until no further increase can be achieved, which results in the partitioned community. The community detection was carried out using the leidenalg package in python (https://leidenalg.readthedocs.io/en/stable/index.html). We performed bootstrapping validation by randomly assigning community partitions and calculating Q values 1000 times. The Q value falling outside the 95% confidence interval suggests the robustness of the community architecture.

E. Statistical Analysis

We conducted the analysis of covariance (ANCOVA) to examine the group differences in morphological features (i.e., SA, CT, CV, and SV) and clinical assessments [i.e., autism diagnostic observation schedule (ADOS) [49]] both between different subtypes and between each subtype and the TDs [Fig. 1(e)]. We converted the ADOS total score (ADOS_TOTAL), communication score (ADOS_COMM), social score (ADOS_SOCIAL), and stereotyped behavior and restricted interest score (ADOS_STEREO_BEHAV) into z-scores to improve their normality. In the ANCOVA model, age, handedness, acquisition site, and the average of the corresponding features across the cortex were included as covariates. Multiple comparisons were corrected by the false discovery rate (FDR) method at the level of $p = 0.05$.

F. Consistency of Subtypes Across Different Age Groups

To explore whether the identified subtypes persist consistently from childhood to adulthood or undergo division and reorganization during this period, we utilized cross-sectional data to fit the development patterns by calculating the distance between each pair of subtypes belonging to the adjacent age groups. Specifically, the mean values of each morphological feature of a younger subgroup were extracted and concatenated to a reference vector of this subtype, and then the distances between the reference vector and the feature vectors of all subjects belonging to an older subgroup were calculated as follows. For example, the distances between the reference vector of a particular subtype of children and the feature vectors of individuals in an adolescent's subtype

$$d_{ij} = \sqrt{\sum_{k=1}^{m}\left(x_{ik} - \overline{y_j}_k\right)^2} \quad (2)$$

where m indicates the number of the regions; x is the feature vector of subject i belonging to an older subtype; $\overline{y_j}$ is the reference vector of subtype J in younger age group; and d_{ij} denotes the distance between the two vectors. If an older subject showed the shortest distance to a younger subtype, it can be inferred that this subject might have developed from this subtype. Then we counted the proportion of individuals within each older subtype that originated from subtypes of the younger age group.

G. Classification Model of ASD Based on Biological Subtypes

We applied five conventional classifiers, including support vector machine (SVM), logistic regression (LR), random forest (RF), gradient boosting tree (GBT), and K-nearest neighbor (KNN), to examine the effect of subtyping on ASD diagnosis [Fig. 1(f)]. The classifiers were trained based on the morphological features of all the ASD and TD individuals as shown in Table I, and were validated on individuals who were excluded from the above analysis because of the small sample size (<10) of the corresponding acquisition site. Detailed information regarding the testing dataset is given in Table S3. Notably, subjects in the testing set also met the criteria (1–4) as mentioned in Section II-A. We performed ANCOVA on the training set to select features with statistical group differences (with $p < 0.05$). The selected features were then used for classification. We constructed subtype-specific classifiers for each age group. A subject showing the highest similarity with the averages of a specific subtype indicated that this subject belongs to said subtype, and should use the specific classifier for this subtype. In addition, the accuracy, sensitivity, specificity, and AUC (area under the receiver operating characteristic curve) were employed to assess the performance of the classifiers.

III. Results

A. Identification of Age-Related ASD Subtypes

Results from the bootstrapping test revealed that Q-values of all community detection tasks, including various feature combinations within each of the three age groups, exceeded the 95% confidence interval (Table II), suggesting the presence of noteworthy community structure among ASD patients. Notably, the multilayer network constructed based on CT and CV demonstrated the highest Q values ($Q > 0.3$) across all age groups, indicating high separability between the identified communities. Therefore, we used the double-layer network constructed with CT and CV for further analysis.

We identified three subtypes in each of the three age groups. The proportion of patients composed for the three subtypes of children ($n = 216$), adolescents ($n = 187$), and adults ($n = 112$) were 39%/28%/33%, 19%/32%/49%, and 47%/31%/22%, respectively. In addition, the subtypes within each age group showed comparable IQ (ANOVA, $p > 0.05$).

B. Comparisons of Morphological Features

Fig. 2 illustrates the comparisons of morphological features between ASD subtypes and the TDs identified in the children group. In particular, subtype 1 showed significantly decreased CT and CV primarily in prefrontal and parietal cortex when

TABLE II
MODULARITY (Q) VALUES OF MULTIPLEX NETWORKS BASED ON DIFFERENT FEATURE COMBINATIONS

Variables	Children		Adolescents		Adults	
	Q	95% Confidence Interval	Q	95% Confidence Interval	Q	95% Confidence Interval
SV + SA	0.18296	[−0.00432, 0.00292]	0.19613	[−0.00595, 0.00381]	0.18113	[−0.00891, 0.00647]
SV + CT	0.18392	[−0.00548, 0.00406]	0.21668	[−0.00744, 0.00535]	0.22684	[−0.01138, 0.00882]
SV + CV	0.18017	[−0.00525, 0.00347]	0.23333	[−0.00765, 0.00488]	0.21161	[−0.01127, 0.00790]
SA + CT	0.19474	[−0.00594, 0.00441]	0.19513	[−0.00815, 0.00581]	0.23028	[−0.01235, 0.00911]
SA + CV	0.19343	[−0.00616, 0.00401]	0.19746	[−0.00825, 0.00505]	0.22720	[−0.01260, 0.00922]
CT + CV	0.30146	[−0.00671, 0.00504]	0.30215	[−0.00901, 0.00691]	0.33832	[−0.01420, 0.01021]
SV + SA + CT	0.13210	[−0.00450, 0.00261]	0.14983	[−0.00639, 0.00377]	0.16756	[−0.00967, 0.00634]
SV + SA + CV	0.12960	[−0.00465, 0.00245]	0.15933	[−0.00615, 0.00349]	0.14880	[−0.00979, 0.00576]
SV + CT + CV	0.13024	[−0.00491, 0.00304]	0.17494	[−0.00626, 0.00444]	0.19079	[−0.01053, 0.00674]
SA + CT + CV	0.15230	[−0.00557, 0.00342]	0.15424	[−0.00771, 0.00456]	0.22110	[−0.01172, 0.00747]
SA + CT + CV + SV	0.10479	[−0.00443, 0.00236]	0.13524	[−0.00595, 0.00324]	0.15129	[−0.00993, 0.00460]

SV, subcortical volume. SA, surface area. CT, cortical thickness. CV, cortical volume. Combination, four-layer multiplex network (SA, CT, CV, and SV).

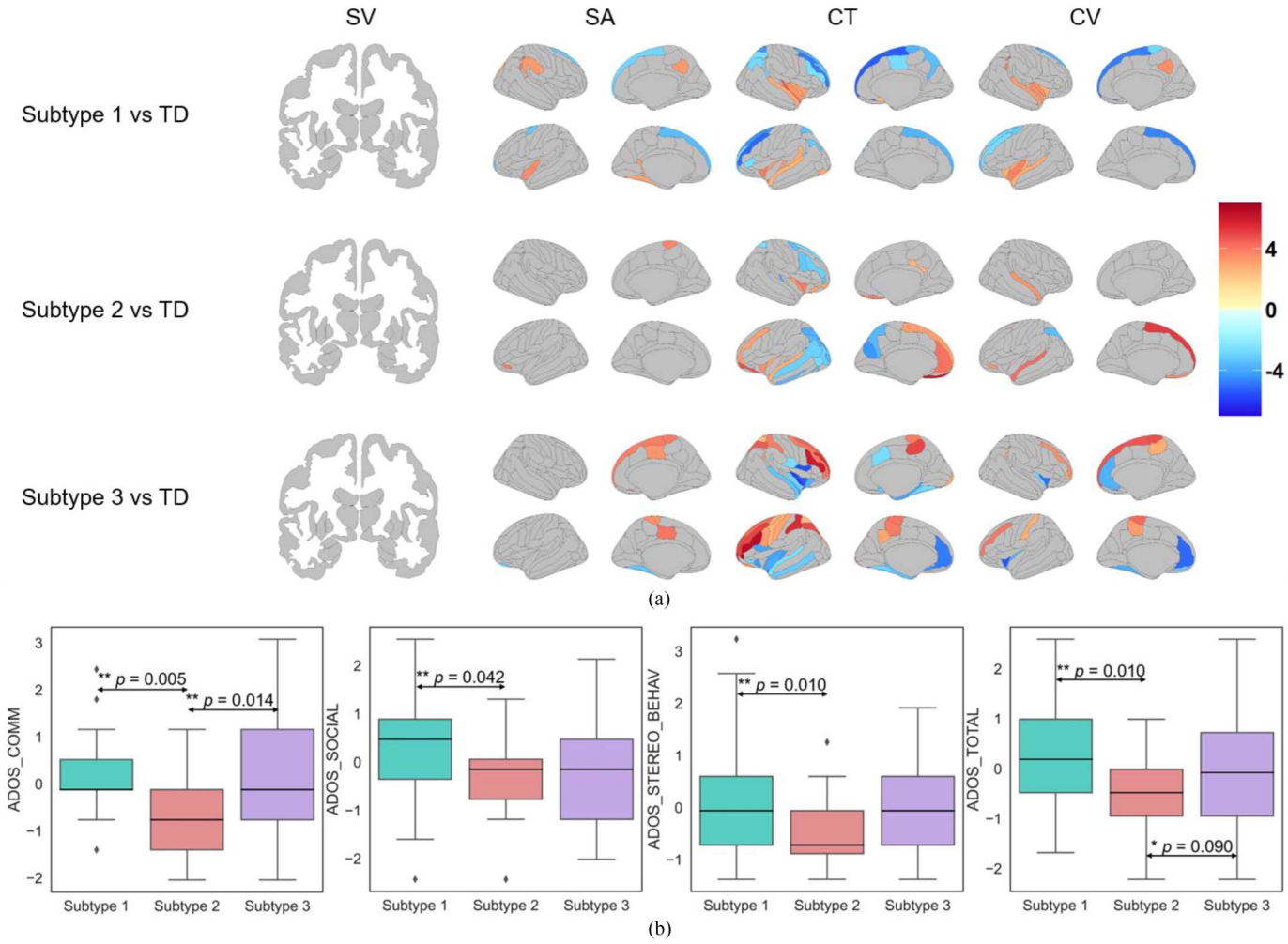

Fig. 2. Comparisons of morphological features and clinical scales between child ASD subtypes and the corresponding TD cohort. (a) Differences in morphological features between ASD children and TDs. The red area indicates that the morphological feature value of this area is higher than that of TD, and the blue area indicates that the morphological feature value of this area is lower than that of TD. (b) Box plots of differences in ADOS clinical scales of ASD patients in children. The four items "ADOS_TOTAL," "ADOS_COMM," "ADOS_SOCIAL," "ADOS_STEREO_BEHAV" of the scale were the z-scores after regressing the covariates (sites, age, handedness, the volume of total gray matters/surface area of white matters/mean cortical thickness/cortex volume) out. **p, p-value with FDR correction which represents significant differences. *p, p-value with FDR correction which represents differences but is not significant. Rhombus, outliers.

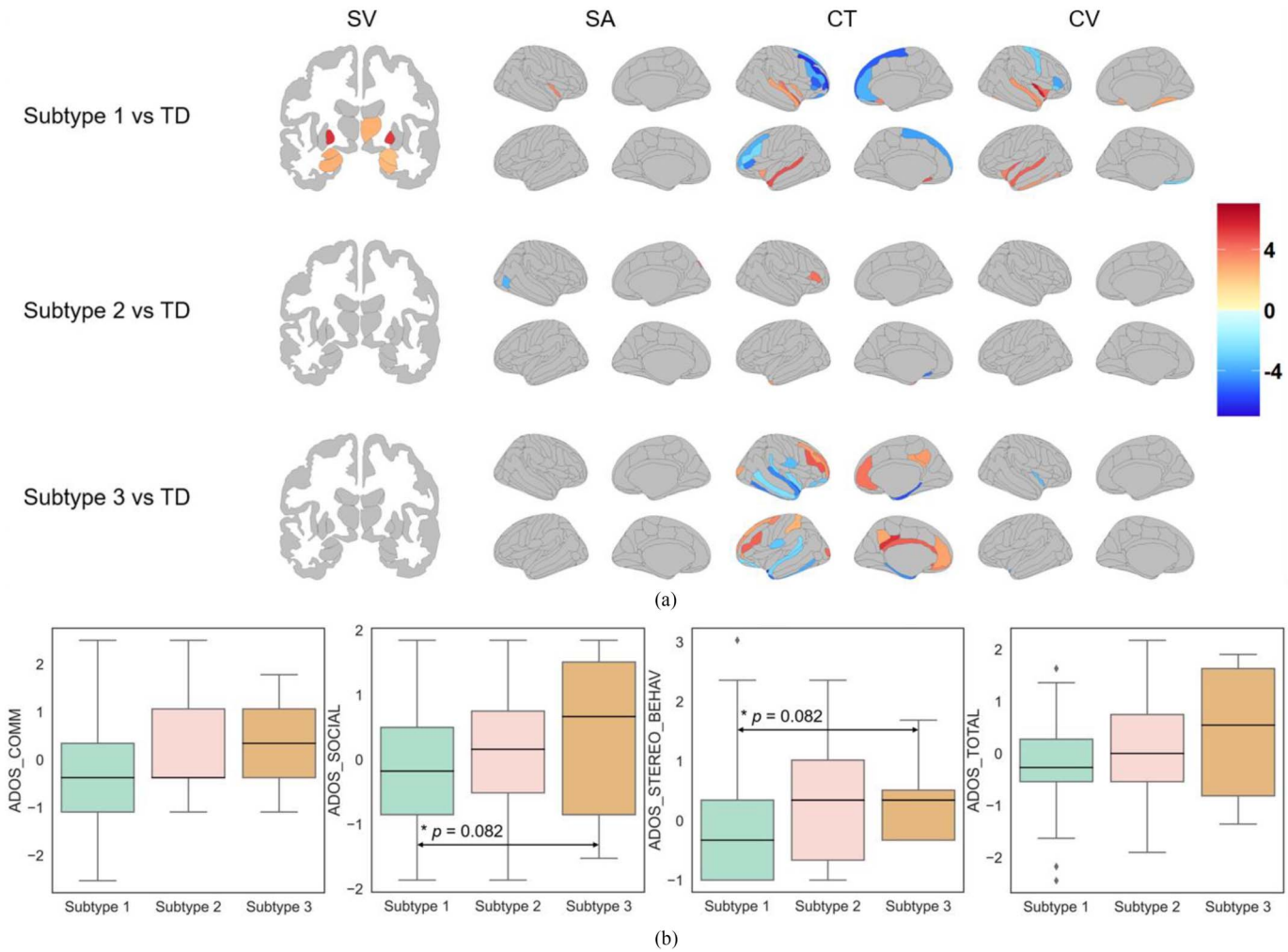

Fig. 3. Comparisons of morphological features and clinical scales between adolescent ASD subtypes and the corresponding TD cohort. (a) Differences in morphological features between ASD and TDs. The red area indicates that the morphological feature value of this area is higher than that of TD, and the blue area indicates that the morphological feature value of this area is lower than that of TD. (b) Box plots of differences in ADOS clinical scales of ASD patients in children. The four items "ADOS_TOTAL," "ADOS_COMM," "ADOS_SOCIAL," "ADOS_STEREO_BEHAV" of the scale were the z-scores after regressing the covariates (sites, age, handedness, the volume of total gray matters/surface area of white matters/mean cortical thickness/cortex volume) out. *p, p-value with FDR correction which represents differences but is not significant. Rhombus, outliers.

compared with the TDs, whereas these features increased in superior temporal gyrus and insula (ANCOVA, FDR corrected $q < 0.05$). The SA of subtype 1 exhibited a similar alteration trend except for the right supramarginal gyrus and subparietal sulcus, which also significantly increased in this cohort relative to the TDs (ANCOVA, FDR corrected $q < 0.05$). Subtype 2 demonstrated more pronounced changes in CT than the other two features compared to the controls, showing significant reductions in left inferior and superior temporal sulcus and right inferior and superior frontal sulcus, and increases in left superior temporal gyrus, left dorsolateral and medial prefrontal cortex (ANCOVA, FDR corrected $q < 0.05$). A similar increasing pattern was also observed in CV. The alterations of CT in subtype 3 were almost opposite to those of subtype 1, showing significant increases in prefrontal cortex and decreases in insula and superior temporal gyrus relative to the TDs (ANCOVA, FDR corrected $q < 0.05$). Moreover, compared to the controls, SA and CV in right dorsomedial prefrontal cortex of subtype 3 increased along with decreased CV in ventromedial prefrontal cortex (ANCOVA, FDR corrected $q < 0.05$). Notably, no significant difference was found in the volumes of subcortical nuclei between each subtype and the TDs (FDR corrected $q > 0.05$). The statistical details of brain regions are given in Tables S4–S7 and the comparisons between subtypes are shown in Fig. S1.

Comparisons of adolescent ASD subtypes and the corresponding TD cohort are visualized in Fig. 3, and the statistical details are given in Tables S4–S7. The alterations of subtype 1 in adolescent patients mirrored those in the subtype 1 of autistic children, showing significant reductions of CT in lateral and medial prefrontal cortex and increases in superior temporal gyrus when compared to the adolescent TDs (ANCOVA, FDR corrected $q < 0.05$). Furthermore, volumes of amygdala, hippocampus, pallidum, and right thalamus also increased in this subtype (ANCOVA, FDR corrected $q < 0.05$). In contrast, the alterations of CT in the aforementioned regions in subtype 3

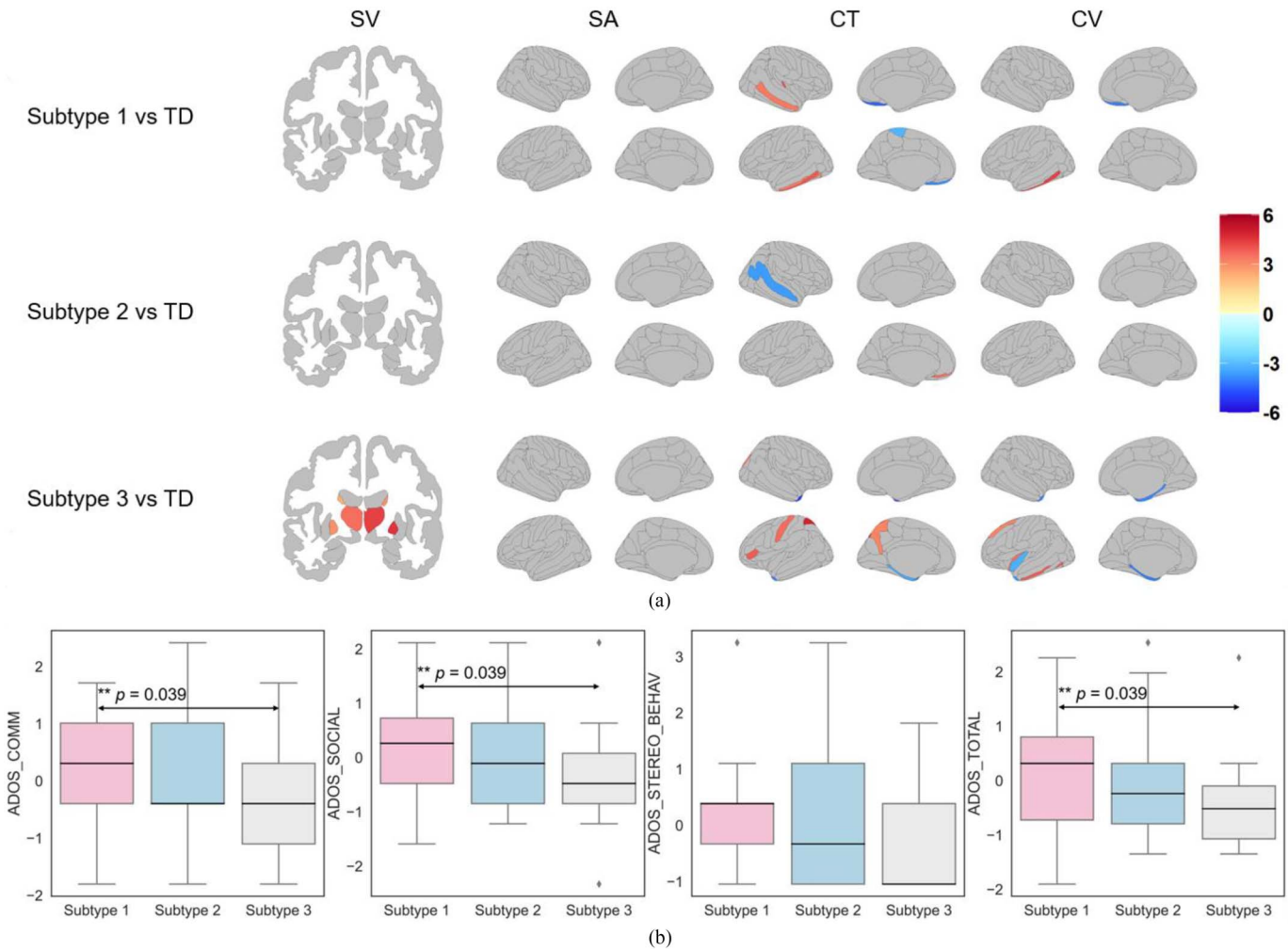

Fig. 4. Comparisons of morphological features and clinical scales between adult ASD subtypes and the corresponding TD cohort. (a) Differences in morphological features between ASD and TDs. The red area indicates that the morphological feature value of this area is higher than that of TD, and the blue area indicates that the morphological feature value of this area is lower than that of TD. (b) Box plots of differences in ADOS clinical scales of ASD patients in children. The four items "ADOS_TOTAL," "ADOS_COMM," "ADOS_SOCIAL," "ADOS_STEREO_BEHAV" of the scale were the z-scores after regressing the covariates (sites, age, handedness, the volume of total gray matters/surface area of white matters/mean cortical thickness/cortex volume) out. **p, p-value with FDR correction which represents significant differences. Rhombus, outliers.

were opposite to subtype 1, except for cingulate and inferior temporal gyrus that exhibiting significant increasing and decreasing trends, respectively, relative to the TDs (ANCOVA, FDR corrected $q < 0.05$). Unlike the other two ASD subtypes in adolescence that exhibiting remarkable cortical changes, subtype 2 only showed significant increase of CT in left subcallosal gyrus and declined SA in right superior occipital gyrus (ANCOVA, FDR corrected $q < 0.05$). The comparisons between the adolescent ASD subtypes are shown in Fig. S2.

Compared with the adult TD group, subtype 1 of ASD adults showed significantly increased CT in right middle and left inferior temporal gyrus and decreased CT in orbital and left paracentral lobule; whereas CT of subtype 2 decreased in superior temporal sulcus (ANCOVA, FDR corrected $q < 0.05$, Fig. 4 and Tables S4–S7). Subtype 3 exhibited significantly increased volumes of thalamus, pallidum, caudate, and left superior frontal and inferior temporal gyrus, increased CT in left Precuneus and central sulcus, and decreased CT and CV in parahippocampal gyrus (ANCOVA, FDR corrected $q < 0.05$, Fig. 4 and Tables S4–S7). The comparisons between the adult ASD subtypes are shown in Fig. S3.

C. Comparisons of Clinical Scales

For the subtypes of children with ASD, the ADOS_TOTAL of subtype 2 was significantly lower than that of subtype 1 and subtype 3 (ANCOVA, FDR corrected $q < 0.05$). The subtype 2 also had significant lower scores in communication, social, and stereotyped behavior than that of subtype 1 [ANCOVA, FDR corrected $q < 0.05$, Fig. 2(b)]. In addition, the communication ability of subtype 3 was better than that of subtype 2, where the statistical difference was marginally significant [ANCOVA, uncorrected $p < 0.05$, Fig. 2(b)]. No significant differences were found in the ADOS scores among the three subtypes of adolescent patients [ANCOVA, FDR corrected $q < 0.05$, Fig. 3(b)]. For the adult subtypes, subtype 1 showed significant higher

Children \ Adolescents	Subtype 1 (92)	Subtype 2 (60)	Subtype 3 (35)
Subtype 1	56 (60.87%)	44 (73.33%)	25 (71.43%)
Subtype 2	33 (35.87%)	9 (15.00%)	3 (8.57%)
Subtype 3	3 (3.26%)	7 (11.67%)	7 (20.00%)

Adolescents \ Adults	Subtype 1 (53)	Subtype 2 (35)	Subtype 3 (24)
Subtype 1	24 (45.28%)	20 (57.14%)	22 (91.67%)
Subtype 2	26 (49.06%)	11 (31.43%)	2 (8.33%)
Subtype 3	3 (5.66%)	4 (11.43%)	0

Fig. 5. Consistency of ASD subtypes throughout the development transitions from childhood to adulthood. The number represents how many subjects of a particular subtype in earlier stage have the shortest distance to the subtypes in later stage, and the corresponding possibilities are also given.

scores of ADOS_TOTAL, ADOS_COMM, and ADOS_SOCIAL than subtype 3 [ANCOVA, FDR corrected $q < 0.05$, Fig. 4(b)], whereas no significant differences were found in the ADOS scores between subtype 2 and other two subtypes (ANCOVA, FDR corrected $q > 0.05$).

D. Consistency of ASD Subtypes Across Age Groups

Our results showed that the identified subtypes did not exhibit consistency throughout the development transitions from childhood to adolescence and from adolescence to adulthood. As shown in Fig. 5, among the three adolescent subtypes, 60.87%, 73.33%, and 71.43% of subjects showed the shortest distance with subtype 1 of ASD children, respectively. Besides, 35.87% of ASD adolescents in subtype 1 exhibited morphological alterations similar to those observed in subtype 2 of children. However, subtypes 2 and 3 of autistic children did not show noteworthy similarity with the other two adolescent subtypes. On the other hand, the majority of adult patients (91.67%) in subtype 3 and approximately half of those in the other two adult subtypes (45.28% and 57.14% of subtype 1 and 2, respectively) demonstrated comparable morphological changes with subtype 1 of adolescents. In addition, subtype 3 of adolescent patients did not exhibit remarkable cortical similarity to any of the three adult subtypes. However, calculating the distance between subtypes with cross-sectional data was only a simulation to infer the development trajectory and it cannot reflect the actual neurobiological development patterns across the age stages.

E. Classification Analysis Based on ASD Subtyping

We found that the application of neuroanatomical subtyping significantly enhanced the diagnostic power of ASD across five widely used classifiers (i.e., SVM, LR, RF, GBT, and KNN) when compared to classify the entire ASD cohort (Table III). Substantial improvement can be observed in all the evaluation metrics (i.e., accuracy, sensitivity, specificity, and AUC). The accuracy was increased by 12.49% on average by using the subtype-specific classifier. Among the five classifiers, LR achieved the highest accuracy of 68.6% (AUC = 0.6787) (Table III and Fig. 6), while KNN demonstrated the most notable improvement, with an increase of 14.78% in accuracy.

IV. Discussion

In this study, we constructed a multilayer network model based on two morphological features (CT and CV) to effectively depict morphometric similarity among individuals. By using an unsupervised community detection algorithm, we identified three subtypes with distinct morphological and clinical phenotypes in child, adolescent, and adult cohorts, respectively. We also found that the subtypes did not maintain high consistency across the three developmental periods, but differentiated and reorganized into different subgroups with age growth. More importantly, classifiers tailored to specific subtypes demonstrated a noteworthy enhancement in the classification performance for patients with ASD. These findings suggested that the manifestation of morphological heterogeneity in autistic brains might vary across developmental stages from childhood to adulthood, and emphasized the potential of subtyping to promote the precision diagnosis of ASD.

We utilized multiple morphological features to dissect the heterogeneity of ASD due to the related atypical structural alterations in the brain [50]. Multilayer networks take advantages of describing various interactions in complex systems so that it has the possibility to represent more complementary information, and community detection is a suitable way to carry out unsupervised clustering with multiple networks. These factors enable us to explore heterogeneous subtypes of ASD. Our results have respectively revealed three subtypes in three developmental stages (i.e., childhood, adolescence, and young adulthood), which presented significant differences in morphological features and clinical scales. This is consistent with that previous studies have revealed evidence for the existence of at least two to four ASD subtypes [23], [25]. The diversity in the number of subtypes identified in ASD may result from the differences in methodology confounds, data acquisition, employed features, and age range for investigation.

Different from other relevant studies, we identified the subtypes within different age ranges (i.e., childhood, adolescence, and young adulthood) to better depict the possible alterations of subtypes with development. It is noteworthy that the most significant morphological differences occurred in CT, and CV exhibited a similar altered tendency with CT. In children with ASD, subtype 1 showed a general decreasing trend was observed in the CT of frontal cortex, while the insula and superior temporal gyrus demonstrated increased thickness, consistent with previous research showing a similar alteration mode in the ASD population [21], [51], [52]. Since the middle frontal gyrus is a critical region responsible for attention, working memory, and language processing [53], [54], and the insula plays an important role in emotion, empathy and social cognition [55], [56], and superior temporal gyrus is the critical region for language function [57], [58], these changes may be related to the deficits in high-order cognitive functions (e.g., emotion processing, language, and social cognition) in patients with ASD [59]. Such speculation was partially supported by the changes in

TABLE III
PERFORMANCE OF FIVE CLASSIFICATION ALGORITHMS IN THE ASD IDENTIFICATION MODEL

Algorithms	Entire-Dataset-Oriented Strategy				Subtype-Oriented Strategy			
	Acc	Sensitivity	Specificity	AUC	Acc	Sensitivity	Specificity	AUC
SVM	0.5289	0.6111	0.4629	0.5369	0.6529	0.6111	0.6866	0.6488
LR	0.6033	0.6852	0.5373	0.6112	0.6860	0.6111	0.7463	0.6787
RF	0.5372	0.6481	0.4477	0.5480	0.6612	0.7407	0.5970	0.6689
GBT	0.5207	0.6852	0.3881	0.5366	0.6612	0.6667	0.6567	0.6617
KNN	0.4711	0.6296	0.3433	0.4865	0.6198	0.8519	0.4328	0.6423

Acc, accuracy; AUC, (area under curve), the area under the ROC curve surrounded by the coordinate axis; SVM, support vector machine; LR, linear regression; RF, random forest; GBT, gradient boosting tree; KNN, k-nearest neighbor.

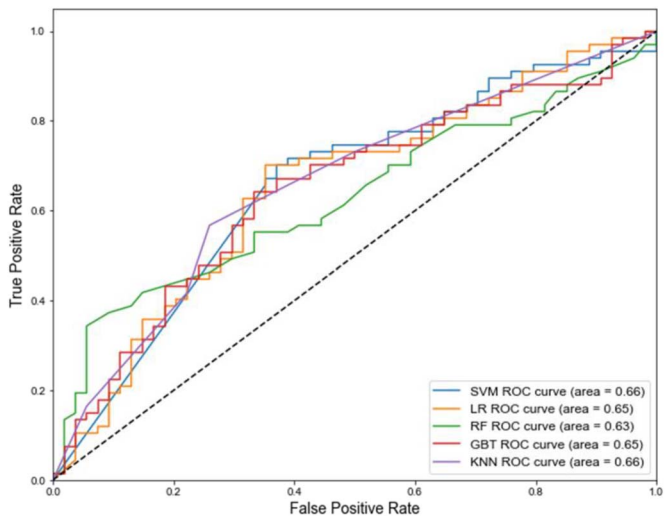

Fig. 6. ROC curves of the five classification algorithms for subtyping-based classification strategy. SVM, support vector machine; LR, logistic regression; RF, random forest; GBT, gradient boosting tree; KNN, k-nearest neighbor. Subtypes, classification based on subtype-specific classifiers. ASD cohort, classification based on the entire ASD cohort.

ADOS scores. Notably, subtype 3 in children showed an opposite changing tendency with subtype 1 in morphological features, which is the thicker middle frontal gyrus and thinner insula and superior temporal gyrus. Although reversed alterations were observed in subtype 1 and subtype 3, both of them showed abnormalities ADOS scores in social and communication scales. Patients in subtype 2 in children presented thicker left superior frontal gyrus, which is important in attitude control, language processing, biological movement, and social information [60]. This was supported by the lower ADOS total and communication score of subtype 2 in child patients. Besides, these findings were consistent the with previous study showing thicker left superior frontal gyrus in autistic children [61]. For the adolescents, we found a similar changing pattern with children in cortex. However, the subcortical nuclei, e.g., amygdala and hippocampus, became larger in subtype 1 of adolescent patients. Both amygdala and hippocampus are known as the important factors in the formation of memory. Moreover, amygdala is considered to be associated with emotion processing [62], [63]. Therefore, the morphological abnormality of amygdala and hippocampus implied impaired cognition and sociability in adolescents with ASD. The alteration patterns of adult ASD subtypes were completely different from those observed in the other two age groups. For instance, the abnormal alterations of insula and prefrontal cortex presented in children and adolescents with ASD were no longer observed in adult patients. This was consistent with prior studies indicating early overgrowth of cerebral cortex in ASD patients [16], [17], [18] and then thin at an accelerated rate after entering adulthood [19], [20]. Furthermore, parts of the temporal lobe, such as temporal gyrus and temporal pole, exhibited morphological changes to varying degrees. Superior temporal gyrus and middle temporal gyrus are responsible for language processing [64], [65], [66], [67]. Temporal pole is also known as important in language processing [68]. In addition, this region involves the functions, such as social and emotional processing [69]. Therefore, these morphological abnormalities may lead to the communication deficits and impairment in social interactions in adults with ASD [70].

For the development of subtypes of ASD patients, we found that several subtypes almost remained consistent across the three age stages. For example, 91.67% of subtype 3 in adults originated from subtype 1 in adolescents, and patients in these two subtypes present larger subcortical structures. However, some subtypes tended to differentiate and reorganize across the lifespan. For instance, subtype 1 in children differentiated into three subtypes in adolescents and subtype 1 in adolescents was mainly reorganized from subtype 1 and 2 in children, which might result in the minor behavior differences in adolescents. This may be caused not only by the neurodevelopment [71] but also by the genetic and environmental factors, and these factors have different influences across the age stages [72]. In addition, interventions for ASD, such as behavioral therapy and pharmacotherapy, may lead to the different abnormalities of morphological and behavioral or recognition characteristics, resulting in the differentiation and reorganization of subtypes.

In this study, we introduced a classification method based on heterogeneous ASD subtypes. The best accuracy reached 68.6%, which was much higher than the accuracy achieved on the entire ASD cohort which was not more than 60%. Previous studies employed the multivariate linear classifier on the entire ABIDE database also showed that the diagnostic accuracy did not exceed 60% [23]. The unsatisfactory classification performance may be due to the heterogeneity in ASD [23]. Here, we showed that the subtyping-based classification strategy significantly enhanced the diagnostic power of ASD, suggesting the impact of anatomical heterogeneity on ASD diagnosis could be

reduced by categorizing patients to different subgroups prior to classification. Moreover, the improved diagnostic performance of multiple classifiers indicated the robustness and generalizability of this strategy, and this could help to obtain more accurate diagnosis information in the early treatment of ASD [73].

There were some limitations in this study. First, the sample size we adopted was limited, especially after dividing the age groups and subtypes, which also resulted in the difficulty in validation. Although we introduced an independent dataset to verify the robustness, a larger data sets still need to be adopted in the follow-up study. Second, we only used cross-sectional data to simulate the developmental transition of ASD subtypes. Although it helped us to demonstrate that the subtypes may not maintain stable across a wide age range, the transition possibility we showed could not reflect the true relationship among subtypes across different age range. Therefore, a more appropriate way is to explore this phenomenon on a longitudinal dataset in the future. In addition, ASD is not only associated with atypical alterations in brain morphology but also affects brain activation [73] and microstructures [74], [75]. Multimodal MRI data may better reveal the subtypes of ASD. Therefore, our future work will place on combining structural and functional MRI to dissect the heterogeneity of ASD.

V. Conclusion

In this study, we conducted community detection with multiplex network composed of the covariance networks of CT and CV to explore the heterogeneity of ASD. We found three neuroanatomical subtypes of ASD in child, adolescent, and adult cohorts, respectively. For each age range, significant differences in cortical morphology and clinical scales were observed between each subtype and the corresponding TD group, as well as between the subtypes. We also found subtypes of ASD tend to reorganize with development rather than consistently persist from childhood to young adulthood. In addition, the identification of ASD with subtype knowledge outperformed the tradition classification strategy on multiple classifiers. These findings dissected the possible anatomical heterogeneity of ASD and its potential application in the precision diagnosis and effective treatment of ASD.

Conflict of Interest

The authors declare no conflict of interest.

Data Availability Statement

We thank the numerous contributors to the Autism Brain Imaging Data Exchange (ABIDE) database for their effort in the collection, organization, and sharing of their datasets. The data that support the findings of this study are openly available in the ABIDE at https://fcon_1000.projects.nitrc.org/indi/abide/abide_I.html.

References

[1] L. J. Camilleri, K. Maras, and M. Brosnan, "Autism spectrum disorder and social story research: A scoping study of published, peer-reviewed literature reviews," *Rev. J. Autism Develop. Disorders*, vol. 9, no. 1, pp. 21–38, 2022.

[2] M. Lai, M. Lombardo, and S. Baron-Cohen, "*Autism*," *Lancet London Engl.*, vol. 383, pp. 896–910, Mar. 2014.

[3] J. Jang et al., "Rates of comorbid symptoms in children with ASD, ADHD, and comorbid ASD and ADHD," *Res. Develop. Disabilities*, vol. 34, no. 8, pp. 2369–2378, 2013.

[4] K. M. Antshel et al., "An update on the comorbidity of ADHD and ASD: A focus on clinical management," *Expert Rev. Neurother.*, vol. 16, no. 3, pp. 279–293, 2016.

[5] M. Yang et al., "Trial selection tensor canonical correlation analysis (TSTCCA) for depression recognition with facial expression and pupil diameter," *IEEE J. Biomed. Health Inform.*, pp. 1–12, Oct. 2023.

[6] M. Yang et al., "Three-stream convolutional neural network for depression detection with ocular imaging," *IEEE Trans. Neural Syst. Rehabil. Eng.*, vol. 31, pp. 4921–4930, 2023.

[7] X. Shan et al., "Mapping the heterogeneous brain structural phenotype of autism spectrum disorder using the normative model," *Biol. Psychiatry*, vol. 91, no. 11, pp. 967–976, 2022.

[8] M. I. Miller, "Computational anatomy: Shape, growth, and atrophy comparison via diffeomorphisms," *NeuroImage*, vol. 23, pp. S19–S33, Jan. 2004.

[9] C. Ecker et al., "Brain surface anatomy in adults with autism: The relationship between surface area, cortical thickness, and autistic symptoms," *JAMA Psychiatry*, vol. 70, no. 1, pp. 59–70, 2013.

[10] C. Ecker, S. Y. Bookheimer, and D. G. Murphy, "Neuroimaging in autism spectrum disorder: Brain structure and function across the lifespan," *Lancet Neurol.*, vol. 14, no. 11, pp. 1121–1134, 2015.

[11] E. Courchesne, R. Carper, and N. Akshoomoff, "Evidence of brain overgrowth in the first year of life in autism," *JAMA*, vol. 290, no. 3, pp. 337–344, 2003.

[12] E. Courchesne et al., "Mapping early brain development in autism," *Neuron*, vol. 56, no. 2, pp. 399–413, 2007.

[13] M. An, "Unusual brain growth patterns in early life in patients with autistic disorder," *Neurology*, vol. 57, pp. 245–254, Jul. 2001.

[14] H. C. Hazlett et al., "Magnetic resonance imaging and head circumference study of brain size in autism: Birth through age 2 years," *Arch. Gen. Psychiatry*, vol. 62, no. 12, pp. 1366–1376, 2005.

[15] H. C. Hazlett et al., "Early brain overgrowth in autism associated with an increase in cortical surface area before age 2 years," *Arch. Gen. Psychiatry*, vol. 68, no. 5, pp. 467–476, 2011.

[16] E. Courchesne, K. Campbell, and S. Solso, "Brain growth across the life span in autism: Age-specific changes in anatomical pathology," *Brain Res.*, vol. 1380, pp. 138–145, Mar. 2011.

[17] N. Lange et al., "Longitudinal volumetric brain changes in autism spectrum disorder ages 6–35 years," *Autism Res.*, vol. 8, no. 1, pp. 82–93, 2015.

[18] E. Redcay and E. Courchesne, "When is the brain enlarged in autism? A meta-analysis of all brain size reports," *Biol. Psychiatry*, vol. 58, no. 1, pp. 1–9, 2005.

[19] B. B. Braden and C. Riecken, "Thinning faster? Age-related cortical thickness differences in adults with autism spectrum disorder," *Res. Autism Spectr. Disorders*, vol. 64, pp. 31–38, Aug. 2019.

[20] D. Van Rooij et al., "Cortical and subcortical brain morphometry differences between patients with autism spectrum disorder and healthy individuals across the lifespan: Results from the ENIGMA ASD Working Group," *Am. J. Psychiatry*, vol. 175, no. 4, pp. 359–369, 2018.

[21] B. S. Khundrakpam et al., "Cortical thickness abnormalities in autism spectrum disorders through late childhood, adolescence, and adulthood: A large-scale MRI study," *Cerebral Cortex*, vol. 27, no. 3, pp. 1721–1731, 2017.

[22] W. Zheng et al., "Developmental pattern of the cortical topology in high-functioning individuals with autism spectrum disorder," *Human Brain Mapping*, vol. 42, no. 3, pp. 660–675, 2021.

[23] S. Haar et al., "Anatomical abnormalities in autism?" *Cerebral Cortex*, vol. 26, no. 4, pp. 1440–1452, 2016.

[24] W. Zheng et al., "Multi-feature based network revealing the structural abnormalities in autism spectrum disorder," *IEEE Trans. Affective Comput.*, vol. 12, no. 3, pp. 732–742, Jul./Sep. 2021.

[25] S.-J. Hong et al., "Toward neurosubtypes in autism," *Biol. Psychiatry*, vol. 88, no. 1, pp. 111–128, 2020.

[26] S. H. Kim, "Decomposing heterogeneity in autism spectrum disorder through neurosubtyping," *Biol. Psychiatry*, vol. 87, no. 12, pp. e37–e38, 2020.

[27] L. Mottron and D. Bzdok, "Autism spectrum heterogeneity: Fact or artifact?" *Mol. Psychiatry*, vol. 25, no. 12, pp. 3178–3185, 2020.

[28] M. Hrdlicka et al., "Subtypes of autism by cluster analysis based on structural MRI data," *Eur. Child Adolescent Psychiatry*, vol. 14, pp. 138–144, Jun. 2005.

[29] H. Chen et al., "Parsing brain structural heterogeneity in males with autism spectrum disorder reveals distinct clinical subtypes," *Human Brain Mapping*, vol. 40, no. 2, pp. 628–637, 2019.
[30] A. M. Reardon et al., "Subtyping autism spectrum disorder via joint modeling of clinical and connectomic profiles," *Brain Connect.*, vol. 12, no. 2, pp. 193–205, 2022.
[31] X. Guo et al., "Inter-individual heterogeneity of functional brain networks in children with autism spectrum disorder," *Mol. Autism*, vol. 13, no. 1, pp. 1–13, 2022.
[32] M. Kivelä et al., "Multilayer networks," *J. Complex Netw.*, vol. 2, no. 3, pp. 203–271, 2014.
[33] S. Lim et al., "Discordant attributes of structural and functional brain connectivity in a two-layer multiplex network," *Sci. Rep.*, vol. 9, no. 1, 2019, Art. no. 2885.
[34] I. Mahjoub, M. A. Mahjoub, and I. Rekik, "Brain multiplexes reveal morphological connectional biomarkers fingerprinting late brain dementia states," *Sci. Rep.*, vol. 8, no. 1, 2018, Art. no. 4103.
[35] J. Chen et al., "IIFDD: Intra and inter-modal fusion for depression detection with multi-modal information from Internet of Medical Things," *Inf. Fusion*, vol. 102, Feb. 2024, Art. no. 102017.
[36] K. S. Aboud et al., "Structural covariance across the lifespan: Brain development and aging through the lens of inter-network relationships," *Human Brain Mapping*, vol. 40, no. 1, pp. 125–136, 2019.
[37] A. M. Dale, B. Fischl, and M. I. Sereno, "Cortical surface-based analysis: I. Segmentation and surface reconstruction," *Neuroimage*, vol. 9, no. 2, pp. 179–194, 1999.
[38] A. M. Dale and M. I. Sereno, "Improved localizadon of cortical activity by combining EEG and MEG with MRI cortical surface reconstruction: A linear approach," *J. Cogn. Neurosci.*, vol. 5, no. 2, pp. 162–176, 1993.
[39] B. Fischl and A. M. Dale, "Measuring the thickness of the human cerebral cortex from magnetic resonance images," *Proc. Nat. Acad. Sci.*, vol. 97, no. 20, pp. 11050–11055, 2000.
[40] A. F. Rosen et al., "Quantitative assessment of structural image quality," *Neuroimage*, vol. 169, pp. 407–418, Apr. 2018.
[41] J. Monereo-Sánchez et al., "Quality control strategies for brain MRI segmentation and parcellation: Practical approaches and recommendations-insights from the Maastricht study," *Neuroimage*, vol. 237, Aug. 2021, Art. no. 118174.
[42] B. Fischl et al., "Whole brain segmentation: Automated labeling of neuroanatomical structures in the human brain," *Neuron*, vol. 33, no. 3, pp. 341–355, 2002.
[43] J. Velázquez et al., "Cortical thickness estimation: A comparison of FreeSurfer and three voxel-based methods in a test–retest analysis and a clinical application," *Brain Topography*, vol. 34, no. 4, pp. 430–441, 2021.
[44] C. Destrieux et al., "Automatic parcellation of human cortical gyri and sulci using standard anatomical nomenclature," *Neuroimage*, vol. 53, no. 1, pp. 1–15, 2010.
[45] P. A. Filipek et al., "The young adult human brain: An MRI-based morphometric analysis," *Cereb Cortex*, vol. 4, no. 4, pp. 344–360, 1994.
[46] V. A. Traag, L. Waltman, and N. J. Van Eck, "From Louvain to Leiden: Guaranteeing well-connected communities," *Sci. Rep.*, vol. 9, no. 1, pp. 5233, 2019.
[47] V. D. Blondel et al., "Fast unfolding of communities in large networks," *J. Stat. Mech., Theory Exp.*, vol. 2008, no. 10, p. P10008, 2008.
[48] S.-H. Bae et al., "Scalable and efficient flow-based community detection for large-scale graph analysis," *ACM Trans. Knowl. Discovery Data*, vol. 11, no. 3, pp. 1–30, 2017.
[49] C. Lord et al., "The autism diagnostic observation schedule—generic: A standard measure of social and communication deficits associated with the spectrum of autism," *J. Autism Dev. Disorders*, vol. 30, no. 3, pp. 205–223, 2000.
[50] T. Li et al., "Dissecting the heterogeneous subcortical brain volume of autism spectrum disorder using community detection," *Autism Res.*, vol. 15, no. 1, pp. 42–55, 2022.
[51] L. Shen et al., "Cortical thickness abnormalities in autism spectrum disorder," *Eur. Child Adolescent Psychiatry*, vol. 33, no. 1, pp. 65–77, 2024.
[52] K. A. Doyle-Thomas et al., "Effects of age and symptomatology on cortical thickness in autism spectrum disorders," *Res. Autism Spectr. Disorders*, vol. 7, no. 1, pp. 141–150, 2013.
[53] C. M. Thiel, K. Zilles, and G. R. Fink, "Cerebral correlates of alerting, orienting and reorienting of visuospatial attention: An event-related fMRI study," *NeuroImage*, vol. 21, no. 1, pp. 318–328, 2004.
[54] R. G. Briggs et al., "Anatomy and white matter connections of the middle frontal Gyrus," *World Neurosurgery*, vol. 150, pp. e520–e529, Jun. 2021.
[55] L. Q. Uddin et al., "Structure and function of the human Insula," *J. Clin. Neurophysiol.*, vol. 34, no. 4, pp. 300–306, 2017.
[56] P. G. Gasquoine, "Contributions of the insula to cognition and emotion," *Neuropsychol.o Rev.*, vol. 24, pp. 77–87, Jan. 2014.
[57] E. D. Bigler et al., "Superior temporal gyrus, language function, and autism," *Dev. Neuropsychol.*, vol. 31, no. 2, pp. 217–238, 2007.
[58] H. G. Yi, M. K. Leonard, and E. F. Chang, "The encoding of speech sounds in the superior temporal gyrus," *Neuron*, vol. 102, no. 6, pp. 1096–1110, 2019.
[59] M. Hajri et al., "Cognitive deficits in children with autism spectrum disorders: Toward an integrative approach combining social and non-social cognition," vol. 13, Aug. 2022, Art. no. 917121.
[60] L. Shen et al., "Cortical thickness abnormalities in autism spectrum disorder," *Eur. Child Adolescent Psychiatry*, vol. 33, no. 1, pp. 65–77, Jan. 2024.
[61] A. Raznahan et al., "Mapping cortical anatomy in preschool aged children with autism using surface-based morphometry," *NeuroImage: Clin.*, vol. 2, pp. 111–119, Jan. 2013.
[62] S. Baron-Cohen et al., "The amygdala theory of autism," *Neurosci. Biobehav. Rev.*, vol. 24, no. 3, pp. 355–364, 2000.
[63] C. M. Schumann et al., "The amygdala is enlarged in children but not adolescents with autism; the hippocampus is enlarged at all ages," *J. Neurosci.*, vol. 24, no. 28, pp. 6392–6401, 2004.
[64] L. Papeo, B. Agostini, and A. Lingnau, "The large-scale organization of gestures and words in the middle temporal Gyrus," *J. Neurosci.*, vol. 39, no. 30, pp. 5966–5974, 2019.
[65] C.-H. Lai et al., "Neuro-cognitive differences in semantic processing between native speakers and proficient learners of Mandarin Chinese," *Front. Psychol.*, vol. 12, 2021.
[66] A. M. Proverbio et al., "The role of left and right hemispheres in the comprehension of idiomatic language: An electrical neuroimaging study," *BMC Neurosci.*, vol. 10, no. 1, 2009, Art. no. 116.
[67] H.-O. Karnath, "New insights into the functions of the superior temporal cortex," *Nat. Rev. Neurosci.*, vol. 2, no. 8, pp. 568–576, 2001.
[68] B. Pascual et al., "Large-scale brain networks of the human left temporal pole: A functional connectivity MRI study," *Cerebral Cortex*, vol. 25, no. 3, pp. 680–702, 2013.
[69] I. R. Olson, A. Plotzker, and Y. Ezzyat, "The Enigmatic temporal pole: A review of findings on social and emotional processing," *Brain*, vol. 130, no. 7, pp. 1718–1731, 2007.
[70] L. Campisi et al., "Autism spectrum disorder," *British Med. Bull.*, vol. 127, no. 1, pp. 91–100, 2018.
[71] G. Liu et al., "Two neuroanatomical subtypes of males with autism spectrum disorder revealed using semi-supervised machine learning," *Mol. Autism*, vol. 13, no. 1, p. 9, 2022.
[72] B. Wiśniowiecka-Kowalnik and B. A. Nowakowska, "Genetics and epigenetics of autism spectrum disorder—current evidence in the field," *J. Appl. Genetics*, vol. 60, no. 1, pp. 37–47, 2019.
[73] J. B. Huang Jiashuang et al., "Brain network analysis: Method and application," *J. Data Acquisition Process.*, vol. 36, no. 4, pp. 648–663, 2021.
[74] Q. Dong et al., "Altered relationship between functional connectivity and fiber-bundle structure in high-functioning male adults with autism spectrum disorder," *Brain Sci.*, vol. 13, no. 7, p. 1098, 2023.
[75] Z. Zhang and W. Zheng, "The discriminative power of white matter microstructures for autism diagnosis," *IFAC-PapersOnLine*, vol. 53, no. 5, pp. 446–451, 2020.